© 2014. Published by The Company of Biologists Ltd | Journal of Cell Science (2014) 127, 1406–1416 doi:10.1242/jcs.135228

RESEARCH ARTICLE

Androgen receptor complexes probe DNA for recognition sequences by short random interactions

Martin E. Van Royen[1], Wiggert A. van Cappellen[1,2], Bart Geverts[1,2], Thomas Schmidt[3], Adriaan B. Houtsmuller[1,2,*] and Marcel J. M. Schaaf[4,*,‡]

ABSTRACT

Owing to the tremendous progress in microscopic imaging of fluorescently labeled proteins in living cells, the insight into the highly dynamic behavior of transcription factors has rapidly increased over the past decade. However, a consistent quantitative scheme of their action is still lacking. Using the androgen receptor (AR) as a model system, we combined three different fluorescence microscopy assays: single-molecule microscopy, photobleaching and correlation spectroscopy, to provide a quantitative model of the action of this transcription factor. This approach enabled us to distinguish two types of AR–DNA binding: very brief interactions, in the order of a few hundred milliseconds, and hormone-induced longer-lasting interactions, with a characteristic binding time of several seconds. In addition, freely mobile ARs were slowed down in the presence of hormone, suggesting the formation of large AR–co-regulator complexes in the nucleoplasm upon hormone activation. Our data suggest a model in which mobile hormone-induced complexes of transcription factors and co-regulators probe DNA by briefly binding at random sites, only forming relatively stable transcription initiation complexes when bound to specific recognition sequences.

KEY WORDS: Steroid Receptor, Transcription factor, DNA binding, Single-molecule microscopy, FCS, FRAP

INTRODUCTION

The androgen receptor (AR) is a ligand-activated transcription factor that specifically regulates genes involved in the development and maintenance of the male phenotype; it also plays a role in the growth of prostate cancer. Like all steroid receptors (SRs), the AR has a modular structure composed of an N-terminal domain, a DNA-binding domain (DBD) and a C-terminal ligand-binding domain. Upon activation by agonistic ligand binding, SRs translocate from the cytoplasm to the nucleus where they bind hormone response elements in promoter and enhancer regions of target genes. When bound to the target sequences, SRs initiate the recruitment of specific transcriptional co-regulators, which alter local chromatin structure in order to enhance transcription initiation. Subsequently, the basal transcription machinery is recruited, inducing transcription of target genes (McKenna and O'Malley, 2002).

In the past decade, fluorescent labeling of proteins in living cells and advances in quantitative live-cell microscopy has greatly influenced our view of the organization of nuclear processes. Approaches like fluorescence recovery after photobleaching (FRAP) (Van Royen et al., 2009) and fluorescence correlation spectroscopy (FCS) (Weidtkamp-Peters et al., 2009) have provided novel insights into the mechanism of action of nuclear processes. Initial FRAP studies have revealed unexpectedly high mobilities and the occurrence of only brief immobilization events for proteins involved in many nuclear processes, including DNA replication (Leonhardt et al., 2000), DNA damage repair (Essers et al., 2002; Houtsmuller et al., 1999), gene transcription (Dundr et al., 2002; Kimura et al., 2002; McNally et al., 2000; Schaaf et al., 2006) and RNA processing (Kruhlak et al., 2000; Phair and Misteli, 2000). A multitude of FRAP studies have shown that SRs share this common behavior. Importantly, the observed transient immobilizations appear to be dependent on ligand activation and the DNA-binding ability of receptors, suggesting that activated SRs move freely through the nucleus and are bound to chromatin for only short time periods (Farla et al., 2004; Farla et al., 2005; Klokk et al., 2007; Marcelli et al., 2006; McNally et al., 2000; Meijsing et al., 2007; Mueller et al., 2008; Rayasam et al., 2005; Schaaf and Cidlowski, 2003; Schaaf et al., 2005; Stenoien et al., 2001; van Royen et al., 2007).

Using kinetic modeling, a quantitative analysis of FRAP has been performed in several studies (Farla et al., 2005; Hinow et al., 2006; Mueller et al., 2008; Phair et al., 2004; Sprague et al., 2004). However, because of the large number of variables (e.g. number of binding sites, on- and off-rates, and relative sizes of free and bound fractions), the variety of analytical approaches and the inaccuracy of FRAP at short time intervals, the results of these quantifications have not yet provided a consistent view on transcription factor mobility and the nature and timing of their interactions with DNA (van Royen et al., 2011).

To some extent, this problem can be addressed by a complementary approach. FCS has already been applied to SRs in several studies (Jankevics et al., 2005; Mikuni et al., 2007a; Mikuni et al., 2007b) and, recently, the group of McNally (Stasevich et al., 2010) cross-validated FRAP and FCS measurements on glucocorticoid receptor dynamics. Although the findings obtained with the two approaches were relatively consistent, uncertainties, because of a number of approximations in the FRAP and FCS analyses, call for additional approaches to obtain conclusive knowledge of the nature and dynamics of DNA interaction by nuclear proteins.

The most powerful approach to complement the limitations of both FRAP and FCS is to study protein behavior by

[1]Department of Pathology, Erasmus MC, 3000 CA Rotterdam, The Netherlands. [2]Erasmus Optical Imaging Center, Erasmus MC, 3000 CA Rotterdam, The Netherlands. [3]Physics of Life Processes, Institute of Physics, Leiden University, 2333 C Leiden, The Netherlands. [4]Molecular Cell Biology, Institute of Biology, Leiden University, 2333 C Leiden, The Netherlands.
*These authors contributed equally to this work

‡Author for correspondence (m.j.m.schaaf@biology.leidenuniv.nl)

Received 23 May 2013; Accepted 31 December 2013

Journal of Cell Science

Journal of Cell Science (2014) 127, 1406–1416 doi:10.1242/jcs.135228

single-molecule microscopy (SMM) in living cells. Using a laser-based fluorescence microscopy setup equipped with a high-sensitivity and high-speed charge-coupled device (CCD) camera (Schmidt et al., 1996), SMM has successfully been applied to proteins fused to autofluorescent proteins, like GFP, providing insight into the mobility patterns of several proteins at a time resolution of ~5 ms and a positional accuracy of ~40 nm (de Keijzer et al., 2008; Harms et al., 1999; Iino et al., 2001; Lommerse et al., 2005). Initially, these studies mostly focused on membrane proteins, but in recent years, data on the three-dimensional (3D) mobility of fluorescently labeled proteins in the nuclei of living cells have been extracted using this approach. The intra-nuclear mobility of fluorescently labeled inert proteins, such as streptavidin (Grünwald et al., 2008) and ovalbumin (Speil and Kubitscheck, 2010) was determined, showing that these proteins appear to be immobilized transiently inside the nucleoplasm for ~10–20 ms. The first SMM study on a transcription factor in a living cell was performed on the *lac* repressor in *Escherichia coli* cells, in which brief immobilizations (<5 ms) were also observed (Elf et al., 2007). Recently, the transcription factor STAT1 has been studied using SMM, which revealed that activated STAT1 diffuses freely through the nucleus and is transiently immobilized, showing residence times of up to 5 s (Speil and Kubitscheck, 2010).

In the present paper, we have combined SMM with FRAP and FCS in order to study the intra-nuclear dynamics of the AR in detail. This combination of techniques provides consistent quantitative data on the mobility pattern of AR in the nucleus. Our results show the occurrence of a freely diffusing fraction and two different binding events, representing sequence-specific and nonspecific DNA binding. The combination of these three techniques enables the determination of the relative size of the different fractions, the diffusion coefficient of freely moving molecules and binding residence times.

RESULTS

Analysis of single YFP dynamics in 3D

In order to validate our methods for detecting molecules and analysis of the dynamic behavior in a 3D environment, we first studied the free diffusion of yellow fluorescent protein (YFP) in a 50% glycerol solution. Images of this solution, which were captured using an SMM setup (Schmidt et al., 1996), showed individual fluorescence intensity peaks (Fig. 1A) representing single molecules, identified because they fitted well to a Gaussian distribution with an intensity and width similar to single YFP fluorescence intensity peaks previously observed using an identical setup (Harms et al., 2001; Lommerse et al., 2004; Schaaf et al., 2009). The observed signal-to-noise ratio, defined as the fluorescence intensity of an individual fluorophore divided by the standard deviation of the background signal, was ~17, resulting in a positional accuracy of the localization of these individual molecules of ~33 nm (Schmidt et al., 1996).

Image sequences were acquired using time intervals of 6.25, 12.5 and 25 ms, and protein mobility was analyzed using the Particle Image Correlation Spectroscopy (PICS) analysis method described previously (Fig. 1B–D) (Semrau and Schmidt, 2007). The obtained cumulative distribution function of squared displacements $P_{cum}(l)$ fitted well to a one-population model and, for each time lag used, the mean squared displacement (MSD) was calculated using this fit model (Fig. 1D). These values were plotted as a function of the time lag and the resulting curve showed a straight line, which reflected free diffusion of YFP molecules in the 50% glycerol solution (Fig. 1E) with a diffusion coefficient (D) of 7.35±0.99 μm^2/s (all results are shown as ±s.e.m.). This D is in the range of the expected value (9.4 μm^2/s) for YFP in 50% glycerol, which was determined based on the estimated hydrodynamic radius of YFP, using Eqn 4 (see Materials and Methods). Deviations in temperature, glycerol concentration or in the homogeneity of the solution could underlie the difference between the expected and determined value. Subsequently, we studied the dynamics of YFP-labeled histone protein H2B in the nuclei of living (Hep3B) cells. Histone proteins are known to be stably bound to DNA and are, therefore, predominantly immobile. Similarly to the data on free YFP, the data on H2B-YFP fitted to a one-population model. The MSD plot showed a straight line with a diffusion coefficient ~200-fold lower than that of YFP in 50% glycerol (D=0.040±0.0023 μm^2/s), which probably reflects the slow movement of chromatin in these live nuclei (Fig. 1F).

In silico validation of analysis of 3D protein dynamics

Because we image 2D projections of molecules moving in three dimensions, and the thickness of the 'optical slice' from which this projection is made is limited, one can argue that molecules 'escaping' in the z-direction create a bias in our analysis. To determine the potential limitations of our analysis, we generated data in a series of Monte Carlo simulations and studied whether the optical slice thickness affected the analysis of molecular dynamics (see supplementary material Figs S1, S2). The results of these *in silico* experiments showed that our approach is well suited for analysis of 3D dynamics of a single fraction of freely diffusing molecules (D=0–10 μm^2/s) (supplementary material Fig. S1). In addition, when an immobile fraction was introduced, the simulations demonstrated that molecular dynamics can still be accurately determined using our approach when the immobile fraction was determined at the shortest time lag used (6.25 ms) (supplementary material Fig. S2).

Quantitative analysis of individual AR dynamics

To obtain a detailed description of the dynamic nuclear behavior of ARs in living cells, we applied SMM to Hep3B cells stably expressing ARs labeled with YFP that had been treated with the synthetic AR agonist metribolone (R1881) or the antagonist OH-flutamide (OHF) (Figs 2, 3). Unlike the data for YFP and H2B–YFP, the cumulative distribution function $P_{cum}(l)$ of the ARs best fitted a two-population model (Fig. 3A). From this, the relative fraction size (α) and their mean squared displacements (MSD_1 and MSD_2) were determined and plotted as a function of the time lag.

For wild-type AR in the presence of R1881, the size of the fast fraction was found to be 46.0%±2.9 (Fig. 3B; Table 1). The MSDs of the fast and slow fraction plotted against the time lag fitted to a straight line, indicating free diffusion of both fractions through the nucleus at this timescale (Fig. 3C,D). The diffusion coefficient of the fast fraction (D_1) was calculated to be 1.13±0.09 μm^2/s (Fig. 3G; Table 1), whereas the diffusion coefficient for the slow fraction (D_2) was 0.056±0.003 μm^2/s (Fig. 3H; Table 1). The latter diffusion coefficient is in the same range as that found for H2B–YFP, strongly suggesting that this fraction of ARs is bound to chromatin (see also Fig. 1A,C).

To study the role of AR activity on its mobility in more detail, we performed SMM on OHF-bound AR. The size of the fast fraction increased dramatically to 88.5%±2.8 of ARs (Fig. 3B; Table 1). The diffusion coefficient of this fast fraction was higher

Journal of Cell Science (2014) 127, 1406–1416 doi:10.1242/jcs.135228

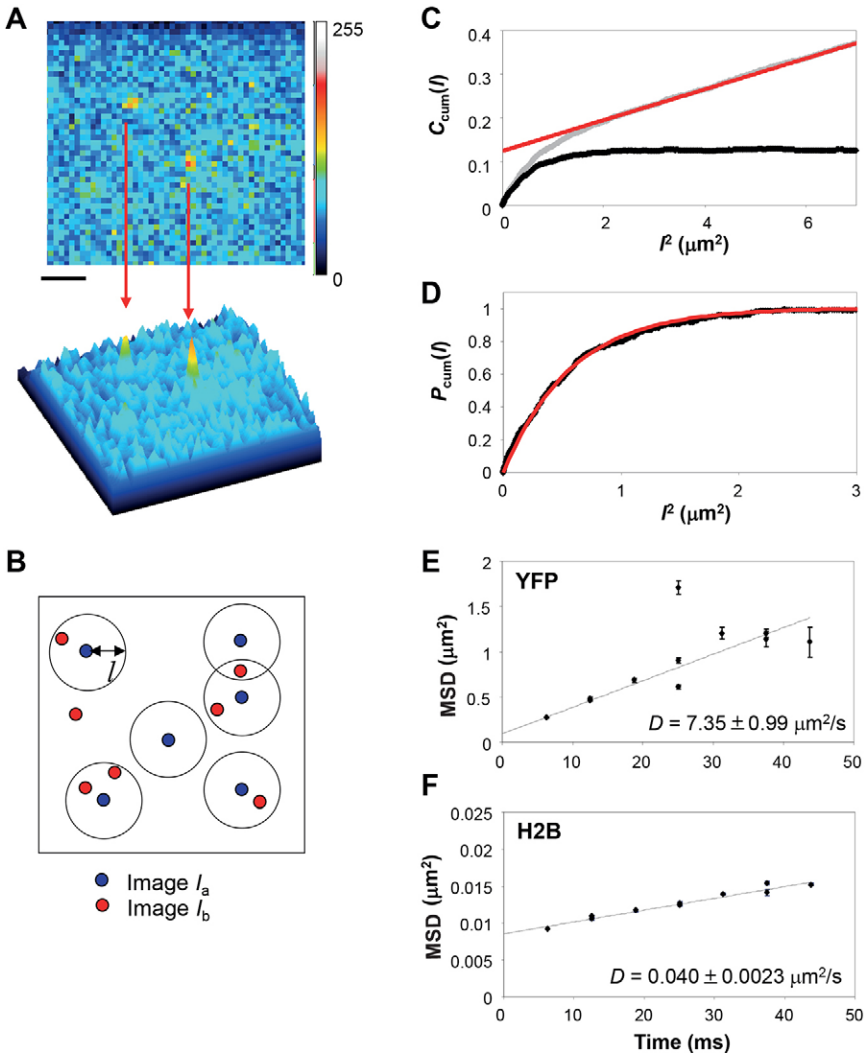

Fig. 1. Single-molecule microscopy and analysis of YFP–AR mobility patterns by particle image correlation spectroscopy. (A) Representative image of YFP molecules in a 50% glycerol solution captured by using the single-molecule microscopy (SMM) setup. Scale bar: 2 μm. The 3D representation of the fluorescence intensities (lower panel) shows two fluorescence intensity peaks that can be attributed to single YFP molecules. (B) Representation of the PICS algorithm (see also Semrau and Schmidt, 2007). For each molecule in image I_a (blue circles), the number of molecules in image I_b (red circles) closer than the length l is counted. In this example, for three molecules in image I_a, one molecule in image I_b closer than l is counted and for two molecules in image I_a two molecules are counted. Thus, a total of seven molecules are counted: five counts are due to diffusion, whereas two counts are a result of random proximity of the molecules. (C) Cumulative correlation function $C_{cum}(l)$. $C_{cum}(l)$ was obtained for individual molecules with a time lag (Δt) of 6.25 ms (gray curve). Subtraction of a correction term derived from a linear fit of the long distance data (red line), representing the contribution of random proximity, yields the cumulative distribution function $P_{cum}(l)$ for the length l of diffusion steps during this time lag (black curve). (D) Curve fitting of $P_{cum}(l)$. Fitting was performed using a monoexponential probability function (red line, Eqn 1), reflecting a one-population model. (E) Mean squared displacement (MSD) of YFP molecules in a 50% glycerol solution, plotted against time. The line represents the curve fit using a free-diffusion model (Eqn 3). The value of the diffusion coefficient D determined this way is indicated. (F). MSD of YFP–H2B in Hep3B cells plotted against time. The line represents the curve fit using a free-diffusion model (Eqn 3). The value of the determined diffusion coefficient D is indicated.

than in the presence of R1881 (2.31±0.10 μm²/s; Fig. 3C,G; Table 1), whereas the diffusion coefficient of the slow fraction was unchanged and in the same range as chromatin-bound H2B (0.063±0.008 μm²/s; Fig. 3D,H).

To verify that the slow fraction of ARs is a result of binding to DNA, an AR was used with a point mutation in the DBD (R585K). This mutant, in which the mutated amino acid is important for base-specific interaction with AR target sequences in DNA (Shaffer et al., 2004), has been found in a patient with complete androgen insensitivity syndrome (Sultan et al., 1993). In line with these findings, it was shown that this AR mutant is transcriptionally inactive (Lobaccaro et al., 1999) and lacks stable binding to DNA (van Royen et al., 2012). Taken together, these data suggest that the R585K mutation disrupts specific interaction of ARs with their target sites in the genome. Like wild-type AR, the AR R585K mutant showed two fractions of molecules. In the presence of the agonist R1881, the size of the fast fraction of mutant ARs (61.1±6.7%; Fig. 3B) was increased as compared with wild-type AR. In addition, the diffusion coefficients of both the fast (1.42±0.08 μm²/s; Fig. 3E,G; Table 1) and the slow fraction (0.077±0.005 μm²/s; Fig. 3F,H; Table 1) were only slightly increased. Thus, the results show that the AR R585K mutant dynamics are only slightly changed as compared with the wild-type receptor, indicating that the mutant is still able to bind to chromatin for periods within the timescale of the experiment (<50 ms).

The presence of the antagonist OHF slightly increased the size of the fast fraction of the mutant AR (79.7±4.0, Fig. 3B) in comparison with R1881, but the difference between R1881 and OHF is remarkably smaller than for the wild-type receptor (Fig. 3B; Table 1). The diffusion coefficient of the slow fraction (0.090±0.013 μm²/s; Fig. 3F,H) was unaltered, whereas the diffusion coefficient of the fast fraction (2.24±0.19 μm²/s; Fig. 3E,G; Table 1) was increased. Apparently, the difference between the sizes of the fast fractions of R1881-bound and OHF-bound wild-type ARs depends on the ability to bind DNA, whereas the difference in diffusion rate of the fast fraction is not dependent on the DNA-binding capacity of AR.

In summary, the results of our SMM experiments indicate the presence of two AR fractions, that both show free diffusion through the nucleus at the timescale of our experiments. The diffusion coefficient of the slow fraction is ~20-fold lower than that of the fast fraction. Treatment with an antagonist dramatically decreased the size of the slow fraction and increased the diffusion rate of the fast fraction. Interestingly, a mutation in the DBD decreased the difference in the size of the fast fraction between agonist- and antagonist-bound ARs but left the difference in diffusion rate of the fast fraction intact.

Journal of Cell Science (2014) 127, 1406–1416 doi:10.1242/jcs.135228

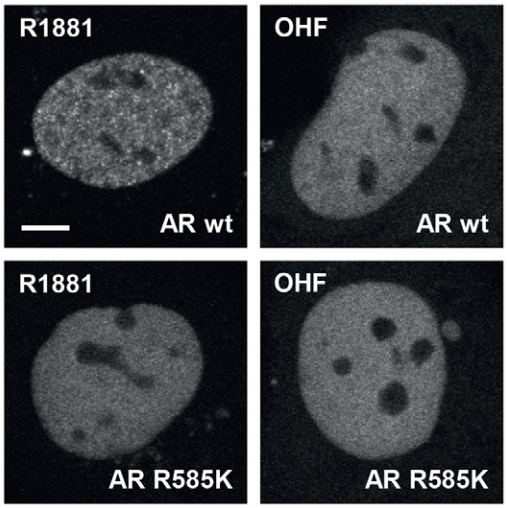

Fig. 2. Confocal images of agonist- and antagonist-bound wild-type and mutant AR. Hep3B cells transiently transfected with YFP labeled ARs. Agonist (R1881)-bound AR shows a typical speckled distribution whereas the mutant AR R585K, which has a point mutation in the DNA-binding domain disabling interactions with the cognate AR target sequence, is homogeneously distributed in the presence of R1881 (see also van Royen et al., 2012). When bound with antagonist (OHF), both wild-type (wt) and the R585K mutant AR show a more homogeneous distribution. Scale bar: 5 μm.

Combining SMM analysis of ARs with FCS and FRAP

To verify the parameters obtained by SMM and expand the timescale of measurements on the dynamic behavior of the AR, the cell lines stably expressing AR–YFP and its R585K mutant, which had been used in the single-molecule analysis, were subjected to both FCS and FRAP (Figs 4 and 5, respectively). For accurate comparison, it must be noted that the FCS approach used in this study, in which intensity fluctuations are measured for 20 s, does not detect molecules that are immobile for periods in the range of seconds and longer because of photobleaching and the small number of long events in this time frame, and that inaccuracy in FRAP at short time intervals limits the ability to extract diffusion parameters, especially for highly mobile molecules.

Therefore in FCS, diffusion rates were only extracted from the retention times of the YFP tagged molecules in the confocal volume, using a two-population free-diffusion triplet-state model (Fig. 4A; supplementary material Fig. S3). The FCS data showed a lower diffusion coefficient (D) for wild-type AR in the presence of R1881 than in the presence of OHF (1.61 ± 0.26 and 2.42 ± 0.37 $\mu m^2/s$, respectively; Fig. 4B). Although the absolute diffusion rates are slightly lower, they are in the same range as those found with SMM (1.13 ± 0.09 $\mu m^2/s$ and 2.31 ± 0.10 $\mu m^2/s$; Fig. 3G; Table 1). This trend was also observed for the R585K mutant AR, for which the diffusion rates (D) determined using FCS are 1.78 ± 0.19 $\mu m^2/s$ and 2.64 ± 0.39 $\mu m^2/s$ in the presence of R1881 and OHF, respectively (Fig. 4B; supplementary material Fig. S3), and 1.42 ± 0.08 $\mu m^2/s$ and 2.24 ± 0.19 $\mu m^2/s$ in SMM (Fig. 3G; Table 1). Thus, the diffusion rates determined by FCS were consistent with the findings from our single-molecule experiments (Table 1).

Subsequently, FRAP experiments were performed and the resulting FRAP data were fitted to curves obtained using computer modeling described previously (e.g. Farla et al., 2005; Van Royen et al., 2009). The large immobile fractions for agonist-bound wild-type AR found in SMM could not be fully attributed to long immobilization events and required the inclusion of short immobilizations in the model. Note that, in previous reports (Farla et al., 2005), these short immobilizations have been explained by slower diffusion but, in combination with the SMM experiments presented here, this model is no longer sufficient.

The diffusion coefficients obtained using SMM and FCS were averaged and used as fixed parameters in the FRAP analysis, and the curves were fitted to a reaction diffusion model with two immobile fractions, one fraction was previously found to have a long interaction time (Farla et al., 2005) and one additional fraction of ARs that had short interactions with the DNA (Fig. 5; supplementary material Fig. S4). As SMM does not discriminate between these long and short immobilizations because of the temporal resolution of this technique (<50 ms), the sum of the two fractions in the FRAP data corroborates the results from the SMM experiments (Table 1).

FRAP of agonist-bound wild-type AR showed a fraction of ARs ($28\%\pm3$) with a binding time of 8 ± 2 s (Fig. 5B,C). FRAP data of antagonist-bound AR and the AR R585K mutant did not fit well to models that included these immobilizations. Thus, only the agonist-bound wild-type AR displays stable interactions with chromatin. In contrast, for all agonist- and antagonist-bound wild-type AR and AR R585K a substantial fraction (of ~30%) with sub-second binding times (0.5–0.8 s) was found (Fig. 5C).

In summary, FCS confirms that antagonist-bound ARs show a faster diffusion rate in comparison with agonist-bound (wild-type and mutant) ARs. FRAP showed that only a substantially long immobilization was found for agonist bound wild-type AR, whereas an additional, briefly immobilized, fraction is found for all agonist- or antagonist-bound wild-type AR or AR R585K mutant (Table 1).

DISCUSSION

The view on how proteins find their way through the nucleus to identify and bind their target sites in the vast amount of DNA has been subject to intensive discussion (e.g. Erdel et al., 2011; Halford and Marko, 2004; Mueller et al., 2010; Mueller et al., 2008; Phair et al., 2004; Sprague and McNally, 2005; Sprague et al., 2004; van Royen et al., 2011). In a simple model, proteins diffuse freely though the nucleoplasm and find their targets by random collision, resulting in binding to specific and nonspecific binding sites (Gorski et al., 2006; Halford and Marko, 2004; Hoogstraten et al., 2008; Houtsmuller et al., 1999; McNally et al., 2000; Mueller et al., 2008). However, more sophisticated models based on *in vitro* experiments using isolated DNA suggest that proteins slide along the DNA strand (1D diffusion) or over the chromatin surface enabling proteins to bypass obstacles (2D diffusion) (Blainey et al., 2009; Gorman et al., 2007; Kampmann, 2004).

Although live-cell imaging methods, such as FRAP and FCS, have revealed high mobility of nuclear proteins and the very dynamic nature of their interactions with chromatin, a large variation in quantitative estimates of diffusion rates and DNA-binding kinetics still exists (van Royen et al., 2011; and references therein). This variation is mostly caused by differences in the choice of analytical methods and by different assessment of experimental parameters regarding microscopic properties, such as the laser intensity distribution or photophysical properties

Journal of Cell Science (2014) 127, 1406–1416 doi:10.1242/jcs.135228

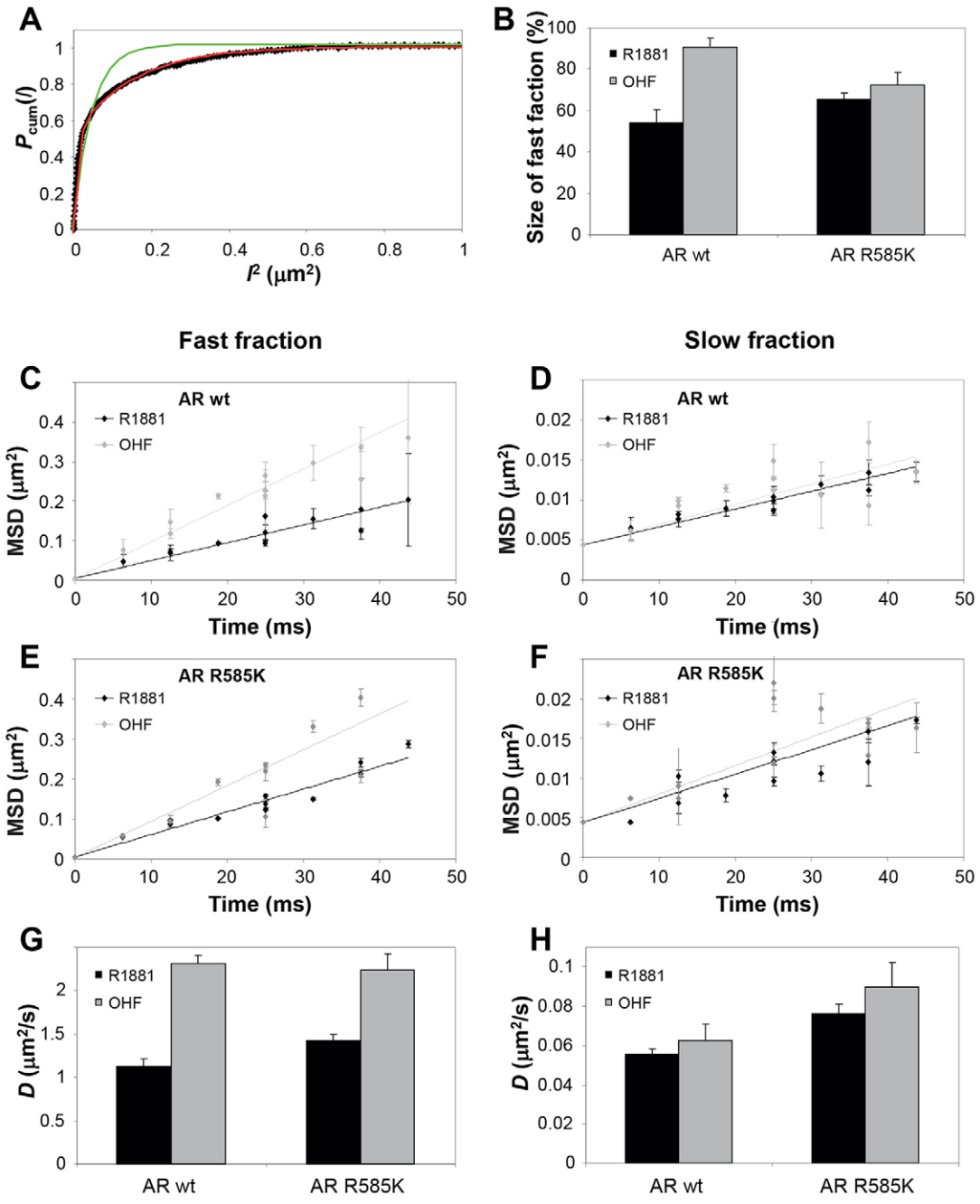

Fig. 3. Quantitative analysis of the dynamic behavior of individual ARs in Hep3B cells by single-molecule microscopy. (A) Cumulative distribution function for individual YFP–AR molecules in the nuclei of Hep3B cells with a time lag Δt of 25 ms (black diamonds). Curves are based on data from three experiments (at least seven cells per experiment), yielding positional data from ~50,000–100,000 fluorescence intensity spots attributed to individual molecules that were analyzed together. Curve fitting was performed using a monoexponential (green line, Eqn 1) and a biexponential (red line, Eqn 2) probability function, reflecting a one- and two-population model, respectively. The results of these fits indicated the occurrence of two fractions of molecules. (B) Relative size of the fast fractions (α) of wild-type YFP–AR and YFP–R585K molecules, in the presence of R1881 and OHF, determined at time lag 6.25 ms. In the presence of OHF the fast fraction is larger than in the presence of R1881. The mutation in the DNA-binding domain results in a slightly increased size of the fast fraction and abolishes the difference between treatment with R1881 and OHF. Two-way ANOVA revealed a significant interaction between the effects of the ligand and the occurrence of the mutation [$F(1,8)=10.7$, $P=0.01$]. (C–F) MSDs of the fast (C,E) and slow (D,F) fraction of YFP–AR (C,D) and YFP–R585K (E,F) molecules plotted against time. Black diamonds show data for molecules in the presence of R1881, gray diamonds show data for molecules in the presence of OHF. Lines represent curve fits using a free diffusion model (Eqn 3, black line represents R1881, gray line represents OHF). Three-way ANOVA of the data of the fast fraction revealed a significant interaction between the effects of the ligand and the time point [$F(6,16)=2.90$, $P=0.04$]. No significant interaction involving the mutation or main effect of the mutation was detected. A similar analysis of the data of the slow fraction revealed a significant interaction between the effects of the ligand and the mutation [$F(1,16)=27.2$, $P<0.0005$]. (G) Diffusion coefficient D of fast fractions obtained using the curve fits shown in C and E. For both the wild-type and the R585K mutant receptor, the diffusion coefficients obtained in the presence of OHF are higher than those obtained in the presence of R1881. (H) Diffusion coefficient D of slow fractions obtained using the curve fits shown in D and F. Diffusion coefficients obtained for the R585K mutant receptor are increased compared with those obtained for the wild-type receptor. The determined positional accuracy (dx) of 33 nm led to a constant offset ($r^2_{(0)}$) in MSD of 0.0044 μm² [$=4\cdot(dx)^2$].

Journal of Cell Science (2014) 127, 1406–1416 doi:10.1242/jcs.135228

Table 1. Detailed quantitative analysis of AR mobility with SMM, FCS and FRAP

			SMM		FCS	FRAP	
			Fraction size (%)	D (μm^2/s)	D (μm^2/s)	Fraction size (%)	Imm. time (s)
AR wt	R1881	Free diff.	46.0±2.9	1.13±0.09	1.61±0.26	38±4	–
		Short imm.	54.0±2.9	0.056±0.003		34±4	0.8±0.2
		Long imm.				28±3	8±2
	OHF	Free diff.	88.5±2.8	2.31±0.10	2.42±0.37	68±5	–
		Short imm.	11.5±2.8	0.063±0.008		32±5	0.5±0.2
		Long imm.				–	–
AR R585K	R1881	Free diff.	61.1±6.7	1.42±0.08	1.78±0.19	66±6	–
		Short imm.	38.9±6.7	0.077±0.005		34±6	0.6±0.3
		Long imm.				–	–
	OHF	Free diff.	79.7±4.0	2.24±0.19	2.64±0.39	71±6	–
		Short imm.	20.3±4.0	0.090±0.013		29±6	0.5±0.2
		Long imm.				–	–

Wt, wild-type; imm, immobilization; diff, diffusion. Results are means±s.e.m.

of fluorescent labels, such as blinking or photobleaching (e.g. Houtsmuller, 2005; Mueller et al., 2012). In addition, differences in the shape and size of the cell nucleus are often not taken into account, even though these might have considerable influence on FRAP recovery curves (as discussed in Houtsmuller, 2005; Mueller et al., 2010; van Royen et al., 2011). Here, we argue that errors caused by such methodological and analytical limitations can be largely eliminated by applying, and using, the strengths of several complementary approaches.

Therefore, we combined FRAP, FCS and SMM to provide a consistent quantitative model of the mobility and DNA interactions of the ligand-dependent transcription factor AR. We obtained mobility and interaction data at different timescales, from milliseconds in FCS, up to tens of milliseconds in single-molecule tracking assays and hundreds of milliseconds to seconds in FRAP. From these data, we determined diffusion rates using FCS and SMM, which gave consistent results (Table 1). In addition, we determined the fraction of immobile molecules using

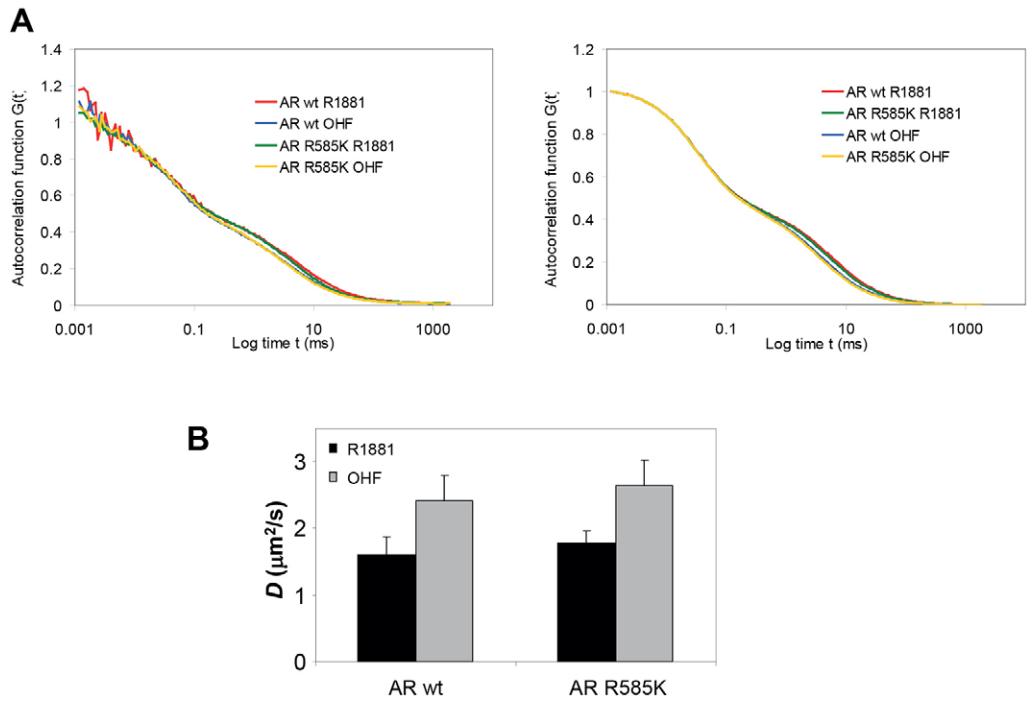

Fig. 4. FCS analysis of YFP-AR dynamics in Hep3B cells. (A) Correlation curves (left panel) and fit curves (right panel) of wild-type and R585K mutant YFP–AR, in the presence of R1881 and OHF. The presented data are averages of at least 100 curves, obtained in three independent experiments in which at least 20 cells were used. Residuals of the fit are shown in supplementary material Fig. S3. The main determinant in these curves appears to be the ligand. The curves for the R585K mutant and the wild-type receptor in the presence of R1881 are similar, as are the two curves generated in the presence of OHF. However, statistical analysis of these data by ANOVA revealed a significant main effect not only of the ligand but also of the mutation, although the latter effect is small [$F(1,100,860)=280.95$, $P<0.0005$, and $F(1,100,860)=38.84$, $P<0.0005$, respectively]. In addition, a significant interaction between the effects of the ligand and the mutation was detected [$F(1,100,860)=24.06$, $P<0.0005$]. (B) Diffusion coefficients of the freely diffusing fraction, determined by fitting of the curves shown in A. Both for the wild-type and the R585K mutant receptor the diffusion coefficients obtained in the presence of OHF are higher than those obtained in the presence of R1881. These data can be compared with those shown in Fig. 3G, which shows the diffusion coefficients of the same fractions determined by SMM.

Journal of Cell Science (2014) 127, 1406–1416 doi:10.1242/jcs.135228

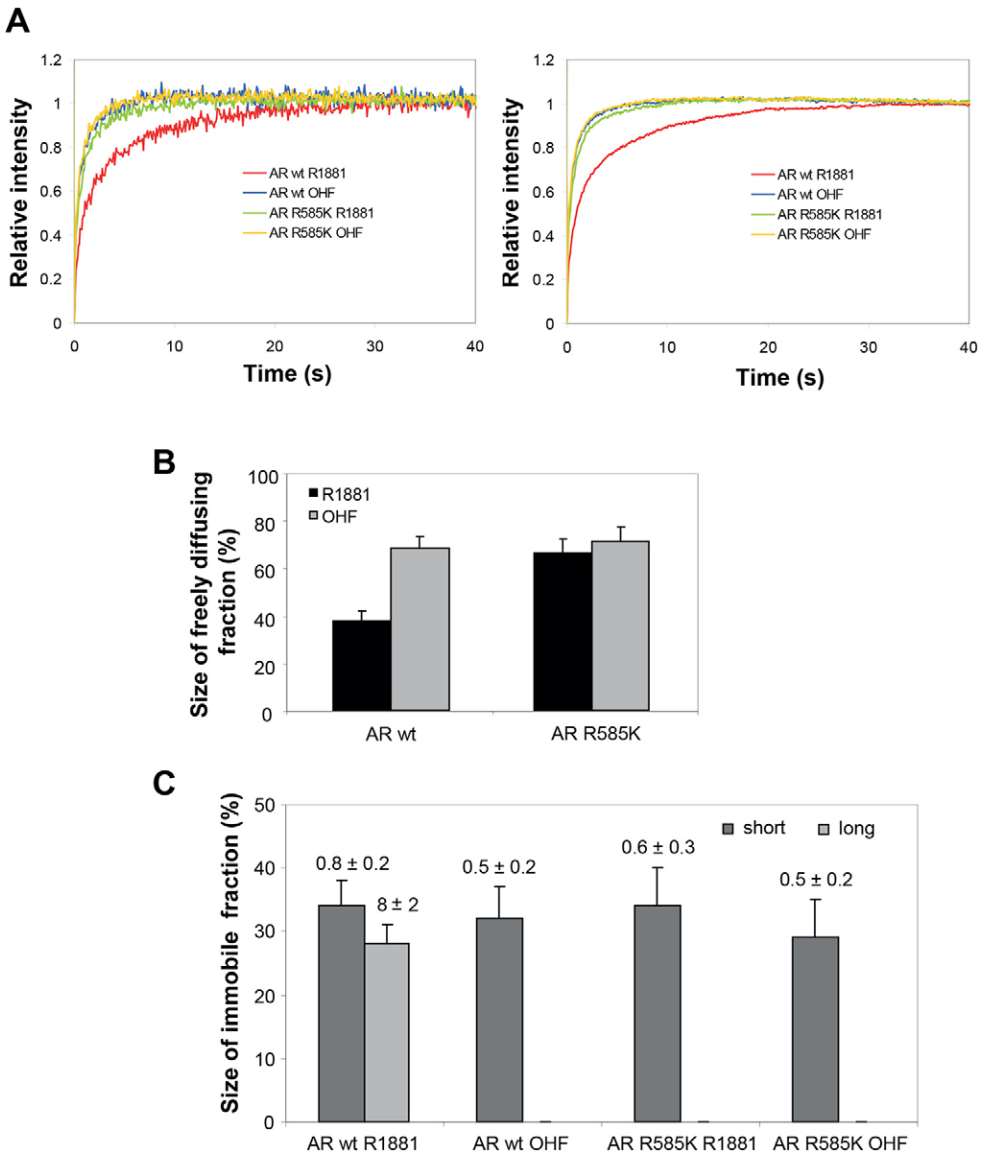

Fig. 5. FRAP analysis of YFP–AR dynamics in Hep3B cells. (A) FRAP curves (left panel) and fit curves (right panel) of wild-type and R585K mutant YFP-AR, in the presence of R1881 and OHF. Residuals of the fit are shown in supplementary material Fig. S4. The FRAP curves represent the average data of at least 25 curves obtained from individual cells in at least two independent experiments. The wild-type receptor in the presence of R1881 shows a slower recovery compared with the other three curves which display similar recovery rates (left panel). Statistical analysis by ANOVA revealed a significant interaction between the effect of the ligand and the mutation [$F(1,54,135)=2675.59$, $P<0.0005$]. These curves were subsequently analyzed quantitatively using Monte Carlo simulations. A large set of simulated FRAP curves were generated and compared with the experimentally generated curves. This way, the size of a freely diffusing fraction, and one or two transiently immobile fraction(s) and their residence times were determined. Curves representing the average parameters of the top 7–10 best fits are presented in the right panel. (B) The relative size of the freely diffusing fraction. The wild-type receptor in the presence of R1881 shows a low fraction size compared with those determined for the other three groups, which display similar fraction sizes. These data can be compared with those shown in Fig. 3B, in which the sizes of the same fractions determined by SMM are shown. Error bars represent 2× s.e.m. (C) Fraction size and residence time of the transiently immobile fraction(s). Data labels represent residence times of the respective fraction. The size of the fraction showing a short immobilization time (0.5–0.8 s) is similar between all groups (~30%), but the wild-type receptor shows an additional fraction with a longer (8 s) residence time.

SMM and FRAP, which also yielded similar results. Further analysis of the FRAP data allowed us to dissect the fraction of immobile molecules into two fractions with distinct kinetics (Table 1).

The results are consistent with a model of activated ARs diffusing freely in the nucleoplasm with frequent, stochastically driven, short binding events, probably representing immobilizations by nonspecific DNA interactions in the sub-second range, as well as less frequent but more stable interactions, typically in the order of tens of seconds (Table 1; Fig. 6). The latter immobilization events most likely represent associations of transcriptionally active ARs with their cognate recognition sequence in promoter and/or enhancer regions of androgen-regulated genes, as these events are absent in an AR mutant (R585K) that is unable to identify its cognate recognition sequences in promoter and/or enhancer regions of androgen-regulated genes (Shaffer et al., 2004). The increased binding stability of wild-type AR might result from the association with stabilizing (co-regulating) factors during formation of transcription complexes or from changes in chromatin structure due to remodeling. This explains the absence of this fraction in the presence of the antagonist OHF, which does not result in binding of these factors (Fig. 6).

As well as the long-binding fraction (~25%), we observed short immobilization events in not only agonist-bound wild-type AR but also in the R585K mutant and antagonist-bound ARs (Table 1). These short immobilizations might reflect a general nonspecific DNA-binding capacity, which is independent of sequence and agonist binding. This behavior could reflect a general mechanism by which nuclear proteins find their target sequences: free 3D diffusion through the nucleus combined with frequent random collisions with chromatin, leading to short interactions. It was previously hypothesized that nuclear proteins repeatedly bind in the same region, interspersed with only short 3D diffusion events to enhance their chances of finding their target sites (sometimes referred to as ‘hopping’ or ‘jumping’), (Gorski et al., 2006; Halford and Marko, 2004; Loverdo et al., 2009; and as previously discussed in van Royen et al., 2011). Although hopping and jumping, indeed, are often described as distinct models, molecules display essentially the same behavior

Journal of Cell Science (2014) 127, 1406–1416 doi:10.1242/jcs.135228

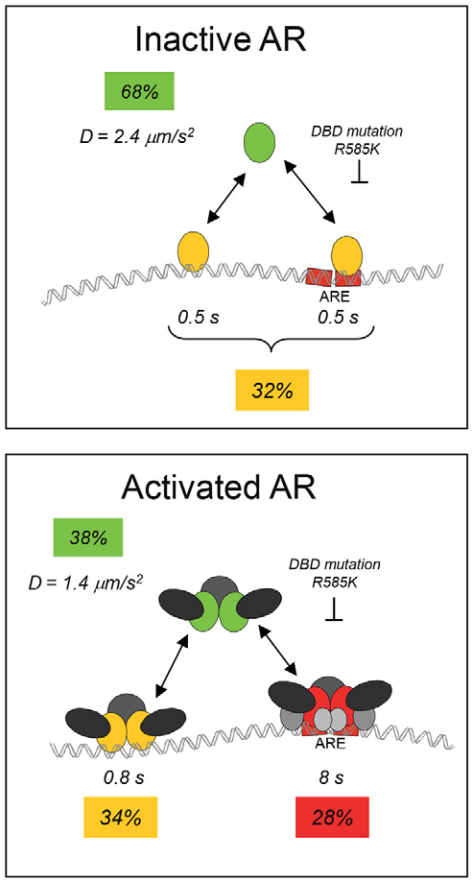

Fig. 6. Kinetic model of nuclear AR. Both ARs bound by antagonist (inactive) or agonist (active) move freely through the nucleoplasm frequently interspersed by short non-sequence-specific interactions with DNA. Only activated ARs show a longer, more stable binding, most likely representing promoter binding. A mutation in the DNA-binding domain disables the longer specific binding events but does not interfere with short interactions with DNA. Activated ARs diffuse more slowly than inactive ARs, indicating that agonist-bound ARs dimerize (van Royen et al., 2012) and are assembled into complexes with cofactors prior to DNA-binding, whereas inactive antagonist-bound ARs remain monomeric. ARE, androgen response element.

in a model of 3D diffusion with random collisions, which is supported by our data. Importantly, because our data fitted well to a model in which the presented diffusion and binding parameters explain the data, it does not suggest the occurrence of 1D diffusion along the DNA helix (‘sliding’). However, the existence of very short 1D sliding behavior over a small distance cannot be ruled out as this might be undetectable by any of the technologies used. Furthermore, AR dimerization does, in theory, allow binding to a distant site that is brought into proximity by the looping of DNA before dissociating from the initial site (‘facilitated diffusion’), but these slowly moving molecules have not been detected by SMM in the present study. Moreover, the crowded nature of regulatory proteins that are bound to DNA will limit the ability of these proteins to scan the DNA for target sites, which by itself makes it an unlikely scenario.

Very recently, it has been reported that (by using a live cell study combining data from SMM, FCS and FRAP experiments) the binding of the transcription factor p53 to DNA showed a continuum in chromatin residence times, which included both sequence-specific and nonspecific binding (Mazza et al., 2012). However, in the present study, two distinct populations of residence times were found for AR, and only the short immobilization was found for the AR mutant R585K (Table 1). Although this seems to present a discrepancy, both studies suggest a very similar model of sequence-specific and nonspecific DNA binding. This is a similar model to that suggested for the *lac* repressor in *E. coli* (Elf et al., 2007). Numerical differences between p53 and AR could be explained by differences in the binding affinity or formation of complexes after binding to DNA.

Interestingly, SMM and FCS consistently indicated a substantial agonist-induced decrease of ~2-fold in the diffusion rate of the freely mobile pool of wild-type and R585K mutant ARs (Table 1). This surprising decrease in diffusion rate could be due the formation of large hormone-induced AR complexes, which diffuse with lower diffusion coefficients (Fig. 6). Because the diffusion coefficient is linearly related to the molecule radius and, therefore, to the cube root of the molecular mass, the observed decrease of a factor of ~1.6 would require a 4-fold increase in the molecular mass of such complexes. It has been shown that ARs dimerize upon agonist binding (van Royen et al., 2012). It is very conceivable that these activated AR dimers associate with a number of co-regulator proteins forming a complex with a molecular mass 4-fold higher than that of the AR monomer, thereby decreasing the diffusion coefficient of this complex 1.6-fold as compared with the AR monomer (Fig. 6). In addition, the data does not exclude the contribution of very brief (≤1 ms) binding events (on top of the previous described short interactions in the 0.5–0.8 ms range) to the diffusion rate decrease. These very short immobilizing interactions, representing an additional scanning behaviour, would be enhanced by agonist binding to result in a lower effective diffusion rate.

In conclusion, combining SMM, FCS and FRAP appears to be a powerful approach to obtain a detailed quantitative description of the dynamic behavior of nuclear proteins in living cells. The results presented here point to a model of free diffusion, where proteins randomly collide with DNA, and two classes of DNA-binding events: relatively long DNA binding, most likely in transcription complexes, and short interactions that might represent search mechanisms.

MATERIALS AND METHODS

Expression constructs and cell culture

The constructs expressing N-terminally YFP-tagged wild-type and mutant AR were generated as described previously (van Royen et al., 2012). In all constructs expressing the AR fusion proteins, the AR was separated from the fluorescent tag by a flexible $(GlyAla)_6$ spacer (Farla et al., 2004). All new constructs were verified by sequencing and the size of expressed ARs was verified by using western blotting. The YFP–H2B expression plasmid was a generous gift from Hiroshi Kimura (Kyoto University, Kyoto, Japan).

Cell lines stably expressing YFP-labeled proteins at very low levels were generated as described previously (Van Royen et al., 2009). Stably expressing cell lines were maintained in α-MEM (Cambrex) supplemented with 5% fetal bovine serum (FBS) (HyClone), 2 mM L-glutamine, 100 µg/ml penicillin, 100 µg/ml streptomycin and 600 µg/ml G418 (active concentration).

Single-molecule microscopy

Cultured Hep3B cells were studied by SMM at 37℃, using a previously described wide-field fluorescence microscopy setup (Harms et al., 2001; Lommerse et al., 2004; Schmidt et al., 1996). The microscope (Axiovert 100TV, Zeiss) was equipped with a 100× oil-immersion objective (NA=1.4, Zeiss). A region of interest was set to 50×50 pixels at a pixel

size of 220 nm. Excitation was performed using a 514-nm argon laser line (Spectra Physics, Mountain View, CA) combined with an acousto-optic tunable filter (AOTF), illuminating the region of interest for 3 ms using a power of ~2 kW/cm^2. The time lag between subsequent illuminations was either 6.25 or 25 ms and the camera frame rate was synchronized with the AOTF. Fluorescent light was filtered using a combination of filters [DCLP530, HQ570/80 (Chroma Technology, Brattleboro, VT) and OG530-3 (Schott, Mainz, Germany)] and detected by a liquid-nitrogen-cooled slow-scan CCD camera (Princeton Instruments, Trenton, NJ).

At least seven cells were studied by taking ten sequences of 120 images in each individual experiment. Positional data from three experiments were pooled for the PICS analysis of the mobility patterns. This way, positional information derived from ~50,000–100,000 fluorescence intensity spots attributed to individual molecules was analyzed as a whole.

Three different time lags were used (6.25, 12.5, and 25 ms). For each time lag, data were obtained for different step sizes in the image sequence (e.g. using a time lag of 6.25 ms, data was obtained for 6.25, 12.5, 18.75, 25, 31.25, 37.5 and 43.75 ms). The generated series of data points ranged from 6.25 to 43.75 ms and for some time-points more than one data point was generated (e.g. the 12.5 ms data point was generated twice, using the 6.25- and 12.5-ms time lag).

Analysis of YFP–AR mobility patterns

Analysis of individual molecules was performed as described previously (Lommerse et al., 2004; Schütz et al., 1997). The signals from fluorescence intensity spots attributed to individual molecules were fitted to a 2D Gaussian surface. This permitted the localization of the molecule with a positional accuracy that is determined by the quotient of the full-width-at-half-maximum of the Gaussian fit and square root of the number of photons detected (Bobroff, 1986).

The 2D mobility patterns were analyzed using the PICS analysis method (Semrau and Schmidt, 2007). Briefly, the cross-correlation between single-molecule positions at two subsequent time-points was calculated (see Fig. 1B). To correct for the effect of random proximity, the contribution from uncorrelated molecules in close proximity (which is described by a linear function) was subtracted (Fig. 1C). This results in the cumulative distribution function $P_{\mathrm{cum}}(l, \Delta t)$ for length l of diffusion steps during time lag Δt (Fig. 1D).

For each time lag P is fitted to one of the following two models (Fig. 1D). The first model is described by the following function:

$$P_{\mathrm{cum}}(l,\Delta t) = 1 - \exp\left(-\frac{l^2}{MSD_0(\Delta t)}\right). \quad (1)$$

It describes the probability that the Brownian particle starting at the origin will be found within a circle of radius l at time lag Δt. It is described by the mean squared displacement $MSD_0(\Delta t)=4\cdot D\cdot\Delta t$. If the population of molecules segregates into two fractions, one with a fast and one with a slow mobility, Eqn 1 becomes:

$$P_{\mathrm{cum}}(l,\Delta t) = 1 - \left[\alpha\cdot\exp\left(-\frac{l^2}{MSD_1(\Delta t)}\right) + (1-\alpha)\cdot\exp\left(-\frac{l^2}{MSD_2(\Delta t)}\right)\right]. \quad (2)$$

This equation describes the second model, characterized by mean squared displacements MSD_1 and MSD_2, and relative fraction α and $(1-\alpha)$, respectively (Schütz et al., 1997). Subsequently, MSD_1 and MSD_2 are plotted against Δt. These plots (Fig. 3C–F) reveal the diffusional behavior of individual fractions.

The plots were best fitted using a free diffusion model:

$$MSD_i(\Delta t) = 4\cdot D_i\cdot\Delta t, \quad (3)$$

in which D_i is the diffusion coefficient. The diffusion coefficient and fraction sizes (±s.e.m.) are given.

The expected diffusion coefficient for YFP in 50% glycerol was determined using the equation:

$$D = \frac{k_B\cdot T}{6\cdot\pi\cdot\eta\cdot r}, \quad (4)$$

in which k_B is the Boltzman constant, T the temperature (25°C), r the hydrodynamic radius of YFP (3 nm), and η the viscosity [$\eta_{\mathrm{H2O:glycerol\ 1:1\ v:v}}$=7.7 centipoise (Cheng, 2008)].

Fluorescence recovery after photobleaching

At least 1 day prior to the experiment, cells stably expressing YFP labeled proteins were plated. The medium was replaced at least 12 h before the experiment by medium with 5% charcoal-stripped FBS, which was supplemented with the appropriate hormone (100 nM R1881 or 1 µM OHF). The quantitative FRAP procedure was performed on a Zeiss LSM510 META confocal laser scanning microscope equipped with a 40×/1.3A NA oil immersion objective, a Lasos LGK 7812ML-4 Laser Class 3B Argon laser (30 mW) and AOTF (Carl Zeiss MicroImaging, Jena, Germany). The temperature was controlled using a heated stage and lens-heating device (37°C). For FRAP analysis a narrow strip spanning the nucleus was scanned at 514 nm excitation with 100 ms intervals at low laser power (Van Royen et al., 2009). Fluorescence intensity of YFP was recorded using a 560-nm longpass filter. After 40 scans, a high-intensity, a 100-ms bleach pulse at 514 nm was applied to photobleach YFP inside the strip. Subsequently, scanning of the bleached strip was continued at 514 nm at low laser intensity. Because of the previously shown absence of a permanently immobile fraction (Farla et al., 2004; Van Royen et al., 2009), the curves were normalized using equation:

$$I_{\mathrm{norm},t} = \frac{(I_t - I_0)}{(I_{\mathrm{final}} - I_0)}, \quad (5)$$

in which I_0 and I_{final} are the fluorescence intensities immediately after the bleach and after complete recovery, respectively.

The FRAP data was quantitatively analyzed by comparing the experimental data with curves generated using Monte Carlo modeling (Van Royen et al., 2009). The computer simulations used to generate FRAP curves for the fit were based on a model that simulates diffusion of molecules and binding to immobile elements in an ellipsoidal volume based on the average size of measured nuclei. The curve generated *in silico* fitting best to an experimental curve under evaluation (by ordinary least squares) was picked from a large set of computer simulated FRAP curves in which two or four parameters representing mobility properties in one or two immobile fractions were varied: fraction sizes (ranging from 0–40%) and the time spent in an immobile state for each fraction (ranging from 0.1–15 s). The diffusion coefficients obtained using SMM and FCS were averaged and used as fixed parameters in this analysis. The laser bleach pulse was simulated based on an experimentally derived 3D laser intensity profile, which was used to determine the probability for each molecule to be bleached according to their 3D position. The simulation used to determine the FRAP curve was run using discrete time steps (Δt) corresponding to the 21-ms experimental scan interval. The number of molecules in the simulations was 10^6, which was empirically determined by producing curves that closely approximate the data with comparable fluctuations. Diffusion was simulated at each new time step $t+\Delta t$ by deriving the new positions ($x_{t+\Delta t}$, $y_{t+\Delta t}$, $z_{t+\Delta t}$) of all mobile molecules from their current positions (x_t, y_t, z_t) by $x_{t+\Delta t}=x_t$ + G(r_1), $y_{t+\Delta t}=y_t$ + G(r_2), and $z_{t+\Delta t}=z_t$ + G(r_3), where r_i is a random number ($0 \le r_i \le 1$) chosen from a uniform distribution and G(r_i) is the inverse of a cumulative Gaussian function with $\mu=0$ and $\sigma^2=2D\Delta t$, where D is the diffusion coefficient. Immobilization was derived from simple binding kinetics described by:

$$\frac{k_{\mathrm{on}}}{k_{\mathrm{off}}} = \frac{F_{\mathrm{imm}}}{F_{\mathrm{mob}}}, \quad (6)$$

where F_{imm} is the relative number of immobile molecules and $F_{\mathrm{mob}}=1-F_{\mathrm{imm}}$. The probability for each particle to become

immobilized (representing chromatin-binding) is defined as:

$$P_{\text{immobilize}} = k_{\text{on}} = \frac{F_{\text{imm}}}{(T_{\text{imm}} \cdot F_{\text{mob}})}, \quad (7)$$

where T_{imm} is the characteristic time spent in the immobile state. The probability to be released is given by:

$$P_{\text{mobilize}} = k_{\text{off}} = \frac{1}{T_{\text{imm}}}, \quad (8)$$

The parameters of the top 7–10 best fitting (least square fitting) were averaged to represent the properties of the molecules in the experimental data (±2×s.e.m.) and to generate the fit curves in Fig. 5A and supplementary material Fig. S4 (for more details see Farla et al., 2004; Van Royen et al., 2009).

Fluorescence correlation spectroscopy

For analysis using FCS, the cells were prepared as described above for FRAP. FCS experiments were performed on a Zeiss LSM510 confocal laser scanning microscope equipped with a Confocor-2 FCS unit (Carl Zeiss MicroImaging, Jena, Germany). The temperature was controlled using a heated stage and a lens-heating device (37°C). After an initial bleaching period of 3 s, the fluorescence intensity at a randomly chosen location in the nucleus was measured five times for 20 s (excitation 514 nm emission longpass filter 560 nm). Data were analyzed with the SSTC data processor (Scientific Software Technologies Center, Minsk, Belarus). The raw data were autocorrelated (Eqn 9); the autocorrelation curves were analyzed as a two-component free diffusion triplet state model to determine the different retention times in the diffraction limited spot (Eqn 10). In this model, the first component reflects YFP blinking (50%, 100 ms, obtained from direct comparison of YFP with GFP, data not shown) and the second component represents free diffusion. From this, the appropriate diffusion time τ and diffusion coefficient D were determined (±s.d.).

$$G(\tau) = \frac{\langle \delta I(t) \cdot \delta I(t+\tau) \rangle}{\langle I(t) \rangle^2}, \quad (9)$$

where $\delta I(t) = I(t) - \langle I(t) \rangle$, is the deviation from the mean intensity

$$G(\tau) = 1 + \frac{1}{\langle N \rangle} \cdot \frac{1 - T + Te^{\tau/\tau_T}}{(1-T)} \sum_i \frac{1}{\left[1 + \frac{\tau}{\tau_{\text{diff},i}}\right] \cdot \sqrt{1 + \left[\frac{\omega_{xy}}{\omega_z}\right]^2 \cdot \frac{\tau}{\tau_{\text{diff},i}}}}, \quad (10)$$

where ω_{xy} and ω_z describe the distance in lateral and axial direction at which the intensity I decays to $I = I_{0,e}^{-2}$ (Rigler et al., 1993).

Statistical analysis

In order to determine the effect of the ligand and the mutation, the fraction sizes determined using SMM in three individual experiments (shown in Fig. 3B) were analyzed using two-way ANOVA. Average MSDs determined using SMM (shown in Fig. 3C–F) were analyzed using three-way ANOVA so the effect of the ligand, the mutation and the time-point was determined. Individual FCS and FRAP curves (of which averages are shown in Figs 4 and 5, respectively) were analyzed using three-way ANOVA in order to determine the effect of the ligand, the mutation and the time-point. In all analyses, interactions between variables were also determined. Statistical significance was accepted at $P < 0.05$.

Competing interests

The authors declare no competing interests.

Author contributions

M.E.v.R., T.S., A.B.H. and M.J.M.S. designed the research. M.E.v.R. and M.J.M.S. performed the experiments. M.E.v.R., W.A.v.C., B.G., T.S., A.B.H. and M.J.M.S. contributed analysis tools and/or analyzed data. M.E.v.R. and M.J.M.S. wrote the paper.

Funding

This work was supported by grants from the Netherlands Organization for Scientific Research (NWO-STW) and the SmartMix Program of The Netherlands Ministry of Economic Affairs and the Ministry of Education, Culture and Science.

Supplementary material

Supplementary material available online at
http://jcs.biologists.org/lookup/suppl/doi:10.1242/jcs.135228/-/DC1

References

Blainey, P. C., Luo, G., Kou, S. C., Mangel, W. F., Verdine, G. L., Bagchi, B. and Xie, X. S. (2009). Nonspecifically bound proteins spin while diffusing along DNA. *Nat. Struct. Mol. Biol.* **16**, 1224-1229.

Bobroff, N. (1986). Position measurement with a resolution and noise-limited instrument. *Rev. Sci. Instrum.* **57**, 1152-1157.

Cheng, N. S. (2008). Formula for the viscosity of a glycerol-water mixture. *Ind. Eng. Chem. Res.* **47**, 3285-3288.

de Keijzer, S., Sergé, A., van Hemert, F., Lommerse, P. H., Lamers, G. E., Spaink, H. P., Schmidt, T. and Snaar-Jagalska, B. E. (2008). A spatially restricted increase in receptor mobility is involved in directional sensing during Dictyostelium discoideum chemotaxis. *J. Cell Sci.* **121**, 1750-1757.

Dundr, M., Hoffmann-Rohrer, U., Hu, Q., Grummt, I., Rothblum, L. I., Phair, R. D. and Misteli, T. (2002). A kinetic framework for a mammalian RNA polymerase in vivo. *Science* **298**, 1623-1626.

Elf, J., Li, G. W. and Xie, X. S. (2007). Probing transcription factor dynamics at the single-molecule level in a living cell. *Science* **316**, 1191-1194.

Erdel, F., Müller-Ott, K., Baum, M., Wachsmuth, M. and Rippe, K. (2011). Dissecting chromatin interactions in living cells from protein mobility maps. *Chromosome Res.* **19**, 99-115.

Essers, J., Houtsmuller, A. B., van Veelen, L., Paulusma, C., Nigg, A. L., Pastink, A., Vermeulen, W., Hoeijmakers, J. H. and Kanaar, R. (2002). Nuclear dynamics of RAD52 group homologous recombination proteins in response to DNA damage. *EMBO J.* **21**, 2030-2037.

Farla, P., Hersmus, R., Geverts, B., Mari, P. O., Nigg, A. L., Dubbink, H. J., Trapman, J. and Houtsmuller, A. B. (2004). The androgen receptor ligand-binding domain stabilizes DNA binding in living cells. *J. Struct. Biol.* **147**, 50-61.

Farla, P., Hersmus, R., Trapman, J. and Houtsmuller, A. B. (2005). Antiandrogens prevent stable DNA-binding of the androgen receptor. *J. Cell Sci.* **118**, 4187-4198.

Gorman, J., Chowdhury, A., Surtees, J. A., Shimada, J., Reichman, D. R., Alani, E. and Greene, E. C. (2007). Dynamic basis for one-dimensional DNA scanning by the mismatch repair complex Msh2-Msh6. *Mol. Cell* **28**, 359-370.

Gorski, S. A., Dundr, M. and Misteli, T. (2006). The road much traveled: trafficking in the cell nucleus. *Curr. Opin. Cell Biol.* **18**, 284-290.

Grünwald, D., Martin, R. M., Buschmann, V., Bazett-Jones, D. P., Leonhardt, H., Kubitscheck, U. and Cardoso, M. C. (2008). Probing intranuclear environments at the single-molecule level. *Biophys. J.* **94**, 2847-2858.

Halford, S. E. and Marko, J. F. (2004). How do site-specific DNA-binding proteins find their targets? *Nucleic Acids Res.* **32**, 3040-3052.

Harms, G. S., Sonnleitner, M., Schütz, G. J., Gruber, H. J. and Schmidt, T. (1999). Single-molecule anisotropy imaging. *Biophys. J.* **77**, 2864-2870.

Harms, G. S., Cognet, L., Lommerse, P. H., Blab, G. A. and Schmidt, T. (2001). Autofluorescent proteins in single-molecule research: applications to live cell imaging microscopy. *Biophys. J.* **80**, 2396-2408.

Hinow, P., Rogers, C. E., Barbieri, C. E., Pietenpol, J. A., Kenworthy, A. K. and DiBenedetto, E. (2006). The DNA binding activity of p53 displays reaction-diffusion kinetics. *Biophys. J.* **91**, 330-342.

Hoogstraten, D., Bergink, S., Ng, J. M., Verbiest, V. H., Luijsterburg, M. S., Geverts, B., Raams, A., Dinant, C., Hoeijmakers, J. H., Vermeulen, W. et al. (2008). Versatile DNA damage detection by the global genome nucleotide excision repair protein XPC. *J. Cell Sci.* **121**, 2850-2859.

Houtsmuller, A. B. (2005). Fluorescence recovery after photobleaching: application to nuclear proteins. *Adv. Biochem. Eng. Biotechnol.* **95**, 177-199.

Houtsmuller, A. B., Rademakers, S., Nigg, A. L., Hoogstraten, D., Hoeijmakers, J. H. J. and Vermeulen, W. (1999). Action of DNA repair endonuclease ERCC1/XPF in living cells. *Science* **284**, 958-961.

Iino, R., Koyama, I. and Kusumi, A. (2001). Single molecule imaging of green fluorescent proteins in living cells: E-cadherin forms oligomers on the free cell surface. *Biophys. J.* **80**, 2667-2677.

Jankevics, H., Prummer, M., Izewska, P., Pick, H., Leufgen, K. and Vogel, H. (2005). Diffusion-time distribution analysis reveals characteristic ligand-dependent interaction patterns of nuclear receptors in living cells. *Biochemistry* **44**, 11676-11683.

Kampmann, M. (2004). Obstacle bypass in protein motion along DNA by two-dimensional rather than one-dimensional sliding. *J. Biol. Chem.* **279**, 38715-38720.

Kimura, H., Sugaya, K. and Cook, P. R. (2002). The transcription cycle of RNA polymerase II in living cells. *J. Cell Biol.* **159**, 777-782.

Klokk, T. I., Kurys, P., Elbi, C., Nagaich, A. K., Hendarwanto, A., Slagsvold, T., Chang, C. Y., Hager, G. L. and Saatcioglu, F. (2007). Ligand-specific dynamics of the androgen receptor at its response element in living cells. *Mol. Cell. Biol.* **27**, 1823-1843.

Kruhlak, M. J., Lever, M. A., Fischle, W., Verdin, E., Bazett-Jones, D. P. and Hendzel, M. J. (2000). Reduced mobility of the alternate splicing factor (ASF)

through the nucleoplasm and steady state speckle compartments. *J. Cell Biol.* **150**, 41-52.
Leonhardt, H., Rahn, H.-P., Weinzierl, P., Sporbert, A., Cremer, T., Zink, D. and Cardoso, M. C. (2000). Dynamics of DNA replication factories in living cells. *J. Cell Biol.* **149**, 271-280.
Lobaccaro, J. M., Poujol, N., Térouanne, B., Georget, V., Fabre, S., Lumbroso, S. and Sultan, C. (1999). Transcriptional interferences between normal or mutant androgen receptors and the activator protein 1 – dissection of the androgen receptor functional domains. *Endocrinology* **140**, 350-357.
Lommerse, P. H., Blab, G. A., Cognet, L., Harms, G. S., Snaar-Jagalska, B. E., Spaink, H. P. and Schmidt, T. (2004). Single-molecule imaging of the H-ras membrane-anchor reveals domains in the cytoplasmic leaflet of the cell membrane. *Biophys. J.* **86**, 609-616.
Lommerse, P. H., Snaar-Jagalska, B. E., Spaink, H. P. and Schmidt, T. (2005). Single-molecule diffusion measurements of H-Ras at the plasma membrane of live cells reveal microdomain localization upon activation. *J. Cell Sci.* **118**, 1799-1809.
Loverdo, C., Bénichou, O., Voituriez, R., Biebricher, A., Bonnet, I. and Desbiolles, P. (2009). Quantifying hopping and jumping in facilitated diffusion of DNA-binding proteins. *Phys. Rev. Lett.* **102**, 188101.
Marcelli, M., Stenoien, D. L., Szafran, A. T., Simeoni, S., Agoulnik, I. U., Weigel, N. L., Moran, T., Mikic, I., Price, J. H. and Mancini, M. A. (2006). Quantifying effects of ligands on androgen receptor nuclear translocation, intranuclear dynamics, and solubility. *J. Cell. Biochem.* **98**, 770-788.
Mazza, D., Abernathy, A., Golob, N., Morisaki, T. and McNally, J. G. (2012). A benchmark for chromatin binding measurements in live cells. *Nucleic Acids Res.* **40**, e119.
McKenna, N. J. and O'Malley, B. W. (2002). Combinatorial control of gene expression by nuclear receptors and coregulators. *Cell* **108**, 465-474.
McNally, J. G., Müller, W. G., Walker, D., Wolford, R. and Hager, G. L. (2000). The glucocorticoid receptor: rapid exchange with regulatory sites in living cells. *Science* **287**, 1262-1265.
Meijsing, S. H., Elbi, C., Luecke, H. F., Hager, G. L. and Yamamoto, K. R. (2007). The ligand binding domain controls glucocorticoid receptor dynamics independent of ligand release. *Mol. Cell. Biol.* **27**, 2442-2451.
Mikuni, S., Pack, C., Tamura, M. and Kinjo, M. (2007a). Diffusion analysis of glucocorticoid receptor and antagonist effect in living cell nucleus. *Exp. Mol. Pathol.* **82**, 163-168.
Mikuni, S., Tamura, M. and Kinjo, M. (2007b). Analysis of intranuclear binding process of glucocorticoid receptor using fluorescence correlation spectroscopy. *FEBS Lett.* **581**, 389-393.
Mueller, F., Wach, P. and McNally, J. G. (2008). Evidence for a common mode of transcription factor interaction with chromatin as revealed by improved quantitative fluorescence recovery after photobleaching. *Biophys. J.* **94**, 3323-3339.
Mueller, F., Mazza, D., Stasevich, T. J. and McNally, J. G. (2010). FRAP and kinetic modeling in the analysis of nuclear protein dynamics: what do we really know? *Curr. Opin. Cell Biol.* **22**, 403-411.
Mueller, F., Morisaki, T., Mazza, D. and McNally, J. G. (2012). Minimizing the impact of photoswitching of fluorescent proteins on FRAP analysis. *Biophys. J.* **102**, 1656-1665.
Phair, R. D. and Misteli, T. (2000). High mobility of proteins in the mammalian cell nucleus. *Nature* **404**, 604-609.
Phair, R. D., Scaffidi, P., Elbi, C., Vecerová, J., Dey, A., Ozato, K., Brown, D. T., Hager, G., Bustin, M. and Misteli, T. (2004). Global nature of dynamic protein-chromatin interactions in vivo: three-dimensional genome scanning and dynamic interaction networks of chromatin proteins. *Mol. Cell. Biol.* **24**, 6393-6402.
Rayasam, G. V., Elbi, C., Walker, D. A., Wolford, R., Fletcher, T. M., Edwards, D. P. and Hager, G. L. (2005). Ligand-specific dynamics of the progesterone receptor in living cells and during chromatin remodeling in vitro. *Mol. Cell. Biol.* **25**, 2406-2418.
Rigler, R., Mets, Ü., Widengren, J. and Kask, P. (1993). Fluorescence correlation spectroscopy with high count rate and low background: analysis of translational diffusion. *Eur. Biophys. J.* **22**, 169-175.
Schaaf, M. J. and Cidlowski, J. A. (2003). Molecular determinants of glucocorticoid receptor mobility in living cells: the importance of ligand affinity. *Mol. Cell. Biol.* **23**, 1922-1934.
Schaaf, M. J. M., Lewis-Tuffin, L. J. and Cidlowski, J. A. (2005). Ligand-selective targeting of the glucocorticoid receptor to nuclear subdomains is associated with decreased receptor mobility. *Mol. Endocrinol.* **19**, 1501-1515.
Schaaf, M. J. M., Willetts, L., Hayes, B. P., Maschera, B., Stylianou, E. and Farrow, S. N. (2006). The relationship between intranuclear mobility of the NF-kappaB subunit p65 and its DNA binding affinity. *J. Biol. Chem.* **281**, 22409-22420.
Schaaf, M. J., Koopmans, W. J., Meckel, T., van Noort, J., Snaar-Jagalska, B. E., Schmidt, T. S. and Spaink, H. P. (2009). Single-molecule microscopy reveals membrane microdomain organization of cells in a living vertebrate. *Biophys. J.* **97**, 1206-1214.
Schmidt, T., Schütz, G. J., Baumgartner, W., Gruber, H. J. and Schindler, H. (1996). Imaging of single molecule diffusion. *Proc. Natl. Acad. Sci. USA* **93**, 2926-2929.
Schütz, G. J., Schindler, H. and Schmidt, T. (1997). Single-molecule microscopy on model membranes reveals anomalous diffusion. *Biophys. J.* **73**, 1073-1080.
Semrau, S. and Schmidt, T. (2007). Particle image correlation spectroscopy (PICS): retrieving nanometer-scale correlations from high-density single-molecule position data. *Biophys. J.* **92**, 613-621.
Shaffer, P. L., Jivan, A., Dollins, D. E., Claessens, F. and Gewirth, D. T. (2004). Structural basis of androgen receptor binding to selective androgen response elements. *Proc. Natl. Acad. Sci. USA* **101**, 4758-4763.
Speil, J. and Kubitscheck, U. (2010). Single ovalbumin molecules exploring nucleoplasm and nucleoli of living cell nuclei. *Biochim. Biophys. Acta* **1803**, 396-404.
Sprague, B. L. and McNally, J. G. (2005). FRAP analysis of binding: proper and fitting. *Trends Cell Biol.* **15**, 84-91.
Sprague, B. L., Pego, R. L., Stavreva, D. A. and McNally, J. G. (2004). Analysis of binding reactions by fluorescence recovery after photobleaching. *Biophys. J.* **86**, 3473-3495.
Stasevich, T. J., Mueller, F., Michelman-Ribeiro, A., Rosales, T., Knutson, J. R. and McNally, J. G. (2010). Cross-validating FRAP and FCS to quantify the impact of photobleaching on in vivo binding estimates. *Biophys. J.* **99**, 3093-3101.
Stenoien, D. L., Patel, K., Mancini, M. G., Dutertre, M., Smith, C. L., O'Malley, B. W. and Mancini, M. A. (2001). FRAP reveals that mobility of oestrogen receptor-alpha is ligand- and proteasome-dependent. *Nat. Cell Biol.* **3**, 15-23.
Sultan, C., Lumbroso, S., Poujol, N., Belon, C., Boudon, C. and Lobaccaro, J. M. (1993). Mutations of androgen receptor gene in androgen insensitivity syndromes. *J. Steroid Biochem. Mol. Biol.* **46**, 519-530.
van Royen, M. E., Cunha, S. M., Brink, M. C., Mattern, K. A., Nigg, A. L., Dubbink, H. J., Verschure, P. J., Trapman, J. and Houtsmuller, A. B. (2007). Compartmentalization of androgen receptor protein-protein interactions in living cells. *J. Cell Biol.* **177**, 63-72.
van Royen, M. E., Farla, P., Mattern, K. A., Geverts, B., Trapman, J. and Houtsmuller, A. B. (2009). Fluorescence recovery after photobleaching (FRAP) to study nuclear protein dynamics in living cells. In *The Nucleus*, Vol. 464 (ed. R. Hancock), pp. 363-385. Totowa, NJ: Humana Press/Springer.
van Royen, M. E., Zotter, A., Ibrahim, S. M., Geverts, B. and Houtsmuller, A. B. (2011). Nuclear proteins: finding and binding target sites in chromatin. *Chromosome Res.* **19**, 83-98.
van Royen, M. E., van Cappellen, W. A., de Vos, C., Houtsmuller, A. B. and Trapman, J. (2012). Stepwise androgen receptor dimerization. *J. Cell Sci.* **125**, 1970-1979.
Weidtkamp-Peters, S., Weisshart, K., Schmiedeberg, L. and Hemmerich, P. (2009). Fluorescence correlation spectroscopy to assess the mobility of nuclear proteins. In *The Nucleus*, Vol. 464 (ed. R. Hancock), pp. 321-341. Totowa, NJ: Humana Press/Springer.